Article

Initial Members of the Family of Molecular Mid-Valent High-Nuclearity Iron Nitrides: [FeNX] and [FeNX] (X = Cl, Br)

Miriam V. Bennett, Sebastian Stoian, Emile L. Bominaar, Eckard Mnck, and Richard H. Holm

J. Am. Chem. Soc., **2005**, 127 (35), 12378-12386• DOI: 10.1021/ja052150l • Publication Date (Web): 13 August 2005

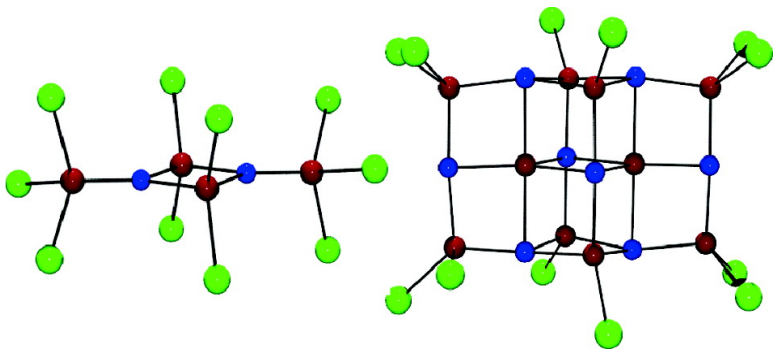

J|A|C|S
ARTICLES
Published on Web 08/13/2005

Initial Members of the Family of Molecular Mid-Valent High-Nuclearity Iron Nitrides: $[Fe_4N_2X_{10}]^{4-}$ and $[Fe_{10}N_8X_{12}]^{5-}$ (X = Cl^-, Br^-)

Miriam V. Bennett,[†] Sebastian Stoian,[‡] Emile L. Bominaar,[‡] Eckard Münck,[‡] and Richard H. Holm*,[†]

Contribution from the Department of Chemistry and Chemical Biology, Harvard University, Cambridge, Massachusetts 02138, and Department of Chemistry, Carnegie Mellon University, Pittsburgh, Pennsylvania 15213

Received April 4, 2005; E-mail: holm@chemistry.harvard.edu

Abstract: Current theoretical and experimental evidence points toward X = N as the identity of the interstitial atom in the $[MoFe_7S_9X]$ core of the iron−molybdenum cofactor cluster of nitrogenase. This atom functions with μ_6 bridging multiplicity to six iron atoms and, if it is nitrogen as nitride, raises a question as to the existence of a family of molecular iron nitrides of higher nuclearity than known dinuclear $Fe^{III,IV}$ species with linear $[Fe-N-Fe]^{5+,4+}$ bridges. This matter has been initially examined by variation of reactant stoichiometry in the self-assembly systems $[FeX_4]^{1-}/(Me_3Sn)_3N$ (X = Cl^-, Br^-) in acetonitrile. A 2:1 mol ratio affords $[Fe_4N_2Cl_{10}]^{4-}$ (**1**), isolated as the Et_4N^+salt (72%). This cluster has idealized C_{2h} symmetry with a planar antiferromagnetically coupled $[Fe^{III}_4(\mu_3\text{-}N)_2]^{6+}$ core containing an Fe_2N_2 rhombus to which are attached two $FeCl_3$ units. DFT calculations have been performed to determine the dominant magnetic exchange pathway. An 11:8 mol ratio leads to $[Fe_{10}N_8Cl_{12}]^{5-}$ (**3**) as the Et_4N^+ salt (37%). The cluster possesses idealized D_{2h} symmetry and is built of 15 edge- and vertex-shared rhomboids involving two μ_3-N and six μ_4-N bridging atoms, and incorporates two of the core units of **1**. Four FeN_2Cl_2 and four FeN_3-Cl sites are tetrahedral and two FeN_5 sites are trigonal pyramidal. The cluster is mixed-valence ($9Fe^{III} + Fe^{IV}$); a discrete Fe^{IV} site was not detected by crystallography or Mössbauer spectroscopy. The corresponding clusters $[Fe_4N_2Br_{10}]^{4-}$ and $[Fe_{10}N_8Br_{12}]^{5-}$ are isostructural with **1** and **3**, respectively. Future research is directed toward defining the scope of the family of molecular iron nitrides.

Introduction

The discovery of a light interstitial atom X (carbon, nitrogen, or oxygen) in the iron−molybdenum cofactor (FeMoco) of nitrogenase by high-resolution X-ray diffraction[1] necessitates a reexamination of certain properties of the cofactor so that the function of this atom may be ascertained. For example, possible biosynthetic pathways to FeMoco must be reformulated,[2,3] and methods for the (as yet unrealized) chemical synthesis[4,5] of the $[MoFe_7(\mu_3\text{-}S)_6(\mu_2\text{-}S)_3(\mu_6\text{-}X)]$ cofactor core must be approached in new ways. Analysis of the electronic parameters of the cofactor in three oxidation states indicates that the interstitial atom is present in all of them and that the likely identity is X = N > C > O.[6] Additional studies using density functional theory concur with nitrogen being the most probable interstitial atom and address the influence of this atom on cofactor properties.[7−11] Nitrogen (as nitride) is located at the center of an Fe_6 trigonal prism with an average Fe−N bond distance of 2.00 Å.[1] Among the questions raised by the putative interstitial nitrogen atom in the context of chemical synthesis are these. Does the atom exert an organizational or template influence on the course of cluster assembly? Given the Fe_6N cofactor fragment, can there exist a family of molecular iron-nitride clusters, and if so, can they be prepared by self-assembly, or are other approaches necessary? Because the probable oxidation states in the resting state of FeMoco are $[Mo^{4+}4Fe^{2+}3Fe^{3+}]$,[6] the molecules of interest would include those with oxidation state $Fe^{\geq 2+}$.

Molecular iron nitrides in the mid- to high-valent range are uncommon. The situation at the outset of this work is summarized in Figure 1, which illustrates two molecular types. Terminal $Fe^{V}{\equiv}N$ species have been detected spectroscopically.[12−15] Two variants of dinuclear bridged species with

[†] Harvard University.
[‡] Carnegie Mellon University.

(1) Einsle, O.; Tezcan, F. A.; Andrade, S. L. A.; Schmid, B.; Yoshida, M.; Howard, J. B.; Rees, D. C. *Science* **2002**, *297*, 1696−1700.
(2) Dos Santos, P. C.; Dean, D. R.; Hu, Y.; Ribbe, M. W. *Chem. Rev.* **2004**, *104*, 1159−1173.
(3) Rubio, L. M.; Ludden, P. W. *J. Bacteriol.* **2005**, *187*, 405−414.
(4) Lee, S. C.; Holm, R. H. *Proc. Natl. Acad. Sci. U.S.A.* **2003**, *100*, 3595−3600.
(5) Lee, S. C.; Holm, R. H. *Chem. Rev.* **2004**, *104*, 1135−1157.
(6) Vrajmasu, V.; Münck, E.; Bominaar, E. L. *Inorg. Chem.* **2003**, *42*, 5974−5988.
(7) Lovell, T.; Liu, T.; Case, D. A.; Noodleman, L. *J. Am. Chem. Soc.* **2003**, *125*, 8377−8383.
(8) Dance, I. *Chem. Commun.* **2003**, 324−325.
(9) Hinnemann, B.; Nørskov, J. K. *J. Am. Chem. Soc.* **2003**, *125*, 1466−1467.
(10) Hinnemann, B.; Nørskov, J. K. *J. Am. Chem. Soc.* **2004**, *126*, 3920−3927.
(11) Dance, I. *J. Am. Chem. Soc.* **2004**, *126*, 11852−11863.
(12) Wagner, W.-D.; Nakamoto, K. *J. Am. Chem. Soc.* **1988**, *110*, 4044−4045.
(13) Meyer, K.; Bill, E.; Mienert, B.; Weyhermüller, T.; Wieghardt, K. *J. Am. Chem. Soc.* **1999**, *121*, 4859−4876.

10.1021/ja052150l CCC: $30.25

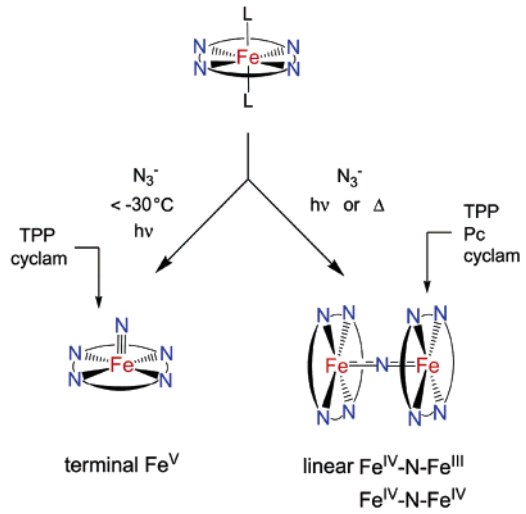

Figure 1. Summary of the two types of molecular iron nitrides known prior to this investigation. As indicated, the large majority were supported by tetraazamacrocyclic ligands (cyclam = 1,4,8,11-tetraazacyclotetradecane, TPP = tetraphenylporphyrinate($^{2-}$), Pc = phthalocyaninate($^{2-}$).

oxidation states $[Fe^{IV}-N-Fe^{III}]^{4+}$ ($S = {}^3/_2$) and $[Fe^{IV}-N-Fe^{IV}]^{5+}$ ($S = 0$) have been prepared and isolated.[16−23] All such species contain linear bridges,[20−26] and the majority of mixed-valence complexes are biased toward a delocalized electronic ground state with iron atoms equivalent by Mössbauer spectroscopy. Such complexes are typified by $[\{Fe(TPP)\}_2N]$, the first molecular iron nitride prepared.[16] We note also the recent report of a terminal $Fe^{IV}\equiv N$ complex and a dinuclear Fe^{II} nonlinear bridged nitride, both of which have phosphine ligands.[27,28] While high-nuclearity iron carbonyls with interstitial nitrogen atoms, including $[Fe_4(\mu_4\text{-}N)(CO)_{12}]^{1-}$,[29] $[Fe_5(\mu_5\text{-}N)(CO)_{14}]^{1-}$,[31] and $[Fe_6(\mu_6\text{-}N)(CO)_{15}]^{3-}$,[32] are well-established, no mid- to high-valent iron nitrides with a nuclearity exceeding two have been reported. Thus far, the most closely related family of Fe^{II}/Fe^{III} clusters are derived from the generalized anions RN^{1-} (R = R′$_2$S, R′$_3$P)[33−37] and RN^{2-} (R = Ar, Bu^t),[38−40] which act as μ_2 or μ_3 bridges in species whose highest nuclearity is four. These clusters appear to follow a pattern of increasing oxidation state and nuclearity with increasing nitrogen atom basicity. The most basic ligand (Bu^tN^{2-}) has been found to form a multiple iron−nitrogen bond.[38] The question arises as to whether iron-nitride clusters can be formed in self-assembly reactions or whether multiple bond formation will intervene, possibly favoring species no larger than dinuclear. The present investigation was undertaken to address the issue of the existence of a family of molecular iron-nitride clusters of higher nuclearity and, ultimately, to ascertain whether their features would be advantageous in the interpretation of cofactor structural and electronic properties. Herein we present the first two structural types within the iron-nitride cluster series together with information on their ground-state electronic structures.

Experimental Section

Preparation of Compounds. All procedures were carried out under a pure dinitrogen atmosphere using standard Schlenk techniques or an inert atmosphere box. All solvents were distilled, deoxygenated, and stored over molecular sieves prior to use. Ether and acetonitrile were passed through an Innovative Technology solvent purification system. THF was distilled from sodium benzophenone ketyl. All compounds were identified by X-ray structure determinations (Table 1). The compounds $(Me_3Sn)_3N$[41] and $(Et_4N)[FeX_4]$ (X = Cl$^-$, Br$^-$)[42] were prepared as described. The Fe^{III} complexes were twice recrystallized from acetonitrile.

$(Et_4N)_4[Fe_4N_2Cl_{10}]$. Neat $(Me_3Sn)_3N$ (0.26 g, 0.52 mmol) was added to a solution of $(Et_4N)[FeCl_4]$ (0.35 g, 1.07 mmol) in 11 mL of acetonitrile, resulting in an immediate color change from pale yellow to black. The solution was stirred for 2 min and allowed to stand for 12 h. After the addition of THF (35 mL), black-orange crystals deposited over 5 h. The crystals were collected, washed with successive aliquots of THF (3 × 10 mL) and ether (2 × 10 mL), and dried in vacuo to give 0.21 g (72%) of product. Absorption spectrum (acetonitrile): λ_{max} (ϵ_M) 292 (30800), 320 (sh, 27500), 540 (sh, 1870), 640 (sh, 1120), 751 (720), 842 (sh, 550) nm. Anal. Calcd for $C_{32}H_{80}Cl_{10}Fe_4N_6$: C, 34.11; H, 7.16; Cl, 31.46; Fe, 19.82; N, 7.46. Found: C, 34.18; H, 7.18; Cl, 31.54; Fe, 19.73; N, 7.37.

$(Et_4N)_4[Fe_4N_2Br_{10}]$. Neat $(Me_3Sn)_3N$ (0.040 g, 0.079 mmol) was added to a solution of $(Et_4N)[FeBr_4]$ (0.090 g, 0.18 mmol) in 3 mL of acetonitrile, resulting in an immediate color change from dark orange to black. The solution was stirred for 30 min and allowed to stand for 8 h. After the addition of THF (25 mL), black, platelike crystals separated over 12 h. The crystals were collected, washed with successive aliquots of THF (3 × 5 mL) and ether (2 × 5 mL), and dried in vacuo to afford 0.037 g (58%) of product. Absorption spectrum (acetonitrile): λ_{max} (ϵ_M) 253 (27000), 266 (sh, 26000), 314 (sh, 23000), 346 (25000), 460 (sh, 6900), 560 (sh, 2100) 665 (sh, 1240), 805 (800) nm.

(14) Grapperhaus, C. A.; Mienert, B.; Bill, E.; Weyhermüller, T.; Wieghardt, K. *Inorg. Chem.* **2000**, *39*, 5306−5317.
(15) Aliaga-Alcalde, N.; George, S. D.; Mienert, B.; Bill, E.; Wieghardt, K.; Neese, F. *Angew. Chem., Int. Ed.* **2005**, *44*, 2908−2912.
(16) Summerville, D. A.; Cohen, I. A. *J. Am. Chem. Soc.* **1976**, *98*, 1747−1752.
(17) Buchler, J. W.; Dreher, C. *Z. Naturforsch.* **1984**, *39b*, 222−230.
(18) Kennedy, B. J.; Murray, K. S.; Homborg, H.; Kalz, W. *Inorg. Chim. Acta* **1987**, *134*, 19−21.
(19) Ercolani, C.; Gardini, M.; Pennesi, G.; Rossi, G.; Russo, U. *Inorg. Chem.* **1988**, *27*, 422−424.
(20) Ercolani, C.; Jubb, J.; Pennesi, G.; Russo, U.; Trigiante, G. *Inorg. Chem.* **1995**, *34*, 2535−2541.
(21) Jüstel, T.; Weyhermüller, T.; Bill, E.; Lengen, M.; Trautwein, A. X.; Hildebrandt, P. *Angew. Chem., Int. Ed. Engl.* **1995**, *34*, 669−672.
(22) Kienast, A.; Homburg, H. *Z. Anorg. Allg. Chem.* **1998**, *624*, 233−238.
(23) Jüstel, T.; Müller, M.; Weyhermüller, T.; Kressl, C.; Bill, E.; Hildebrandt, P.; Lengen, M.; Grodzicki, M.; Trautwein, A. X.; Nuber, B.; Wieghardt, K. *Chem. Eur. J.* **1999**, *5*, 793−810.
(24) Scheidt, W. R.; Summerville, D. A.; Cohen, I. A. *J. Am. Chem. Soc.* **1976**, *98*, 6623−6628.
(25) Moubaraki, P. B.; Benlian, D.; Baldy, A.; Pierrot, M. *Acta Crystallogr.* **1989**, *C45*, 393−394.
(26) Li, M.; Shang, M.; Ehlinger, N.; Schulz, C. E.; Scheidt, W. R. *Inorg. Chem.* **2000**, *39*, 580−583.
(27) Brown, S. D.; Peters, J. C. *J. Am. Chem. Soc.* **2005**, *127*, 1913−1923.
(28) Betley, T. A.; Peters, J. C. *J. Am. Chem. Soc.* **2004**, *126*, 6252−6254.
(29) Fjare, D. E.; Gladfelter, W. L. *J. Am. Chem. Soc.* **1981**, *103*, 1572−1574.
(30) Gourdon, A.; Jeannin, Y. *J. Organomet. Chem.* **1985**, *290*, 199−211.
(31) Hourihane, R.; Spalding, T. R.; Ferguson, G.; Deeney, T.; Zanello, P. *J. Chem. Soc., Dalton Trans.* **1993**, 43−46.
(32) Della Pergola, R.; Bandini, C.; Demartin, F.; Diana, E.; Garlaschelli, L.; Stanghellini, P. L.; Zanello, P. *J. Chem. Soc., Dalton Trans.* **1996**, 747−754.
(33) Roesky, H. W.; Seseke, U.; Noltemeyer, M.; Sheldrick, G. M. *Z. Naturforsch.* **1988**, *43b*, 1130−1136.
(34) Roesky, H. W.; Zimmer, M.; Schmidt, H. G.; Noltemeyer, M. *Z. Naturforsch.* **1988**, *43b*, 1490−1494.
(35) Mai, H.-J.; Wocadlo, S.; Kang, H.-C.; Massa, W.; Dehnicke, K.; Maichle-Mössmer, C.; Strähle, J.; Fenske, D. *Z. Anorg. Allg. Chem.* **1995**, *621*, 705−712.
(36) Riese, U.; Harms, K.; Pebler, J.; Dehnicke, K. *Z. Anorg. Allg. Chem.* **1999**, *625*, 746−754.
(37) LePichon, L.; Stephan, D. W.; Gao, X.; Wang, Q. *Organometallics* **2002**, *21*, 1362−1366.
(38) Verma, A. K.; Nazif, T. N.; Achim, C.; Lee, S. C. *J. Am. Chem. Soc.* **2000**, *122*, 11013−11014.
(39) Link, H.; Decker, A.; Fenske, D. *Z. Anorg. Allg. Chem.* **2000**, *626*, 1567−1574.
(40) Duncan, J. S.; Nazif, T. M.; Verma, A. K.; Lee, S. C. *Inorg. Chem.* **2003**, *42*, 1211−1224.
(41) Sisido, K.; Kozima, S. *J. Org. Chem.* **1964**, *29*, 907−909.
(42) Gill, N. S. *J. Chem. Soc.* **1961**, 3512−3515.

Table 1. Crystallographic Data[a] for Iron-Nitride Clusters[b]

	$(Et_4N)_4$[**1**]	$(Et_4N)_4$[**1**]·2MeCN	$(Et_4N)_4$[**2**]	$(Et_4N)_5$[**3**]·2MeCN	$(Et_4N)_5$[**4**]
formula	$C_{32}H_{80}Cl_{10}Fe_4N_6$	$C_{36}H_{86}Cl_{10}Fe_4N_8$	$C_{32}H_{80}Br_{10}Fe_4N_6$	$C_{44}H_{106}Cl_{12}Fe_{10}N_{15}$	$C_{40}H_{100}Br_{12}Fe_{10}N_{13}$
cryst. syst.	monoclinic	monoclinic	triclinic	orthorhombic	orthorhombic
fw	1126.92	1209.03	1571.52	1826.31	2260.25
space group	$P2_1/n$	$P2_1/c$	$P\bar{1}$	$Aba2$	$Cmcm$
a, Å	13.513(3)	10.064(5)	11.502(3)	43.52(2)	11.514(3)
b, Å	12.731(3)	12.042(6)	11.882(3)	23.303(8)	25.738(5)
c, Å	16.728(4)	24.16(1)	12.206(3)	15.201(5)	25.254(5)
α, deg	90	90	108.305(5)	90	90
β, deg	111.403(4)	90.52(1)	103.908(5)	90	90
γ, deg	90	90	107.892(5)	90	90
V, Å^3	2679(1)	2928(2)	1398.5(6)	15417(9)	7484(3)
Z	2	2	1	8	4
ρ_{calc}, g/cm^3	1.397	1.371	1.866	1.574	2.006
2θ range, deg	4.14 to 56.56	3.38 to 56.64	3.78 to 52.74	1.88 to 57.78	3.16 to 52.92
GOF (F^2)	1.051	0.999	1.033	1.025	1.021
R_1[c]/wR_2[d]%	3.25/7.20	3.60/7.84	2.38/5.21	4.16/9.15	6.27/15.43

[a] Collected using graphite monochromated Mo K_α radiation ($\lambda = 0.71073$ Å) at $T = 193$ K. [b] Designation of clusters: $[Fe_4N_2Cl_{10}]^{4-}$ (1), $[Fe_4N_2Br_{10}]^{4-}$ (2), $[Fe_{10}N_8Cl_{12}]^{5-}$ (3), $[Fe_{10}N_8Br_{12}]^{5-}$ (4). [c] $R_1 = \sum||F_o| - |F_c||/\sum|F_o|$. [d] $wR_2 = \{\sum[w(F_o^2 - F_c^2)^2/\sum[w(F_o^2)^2]\}^{1/2}$.

$(Et_4N)_5[Fe_{10}N_8Cl_{12}]$. Neat $(Me_3Sn)_3N$ (0.56 g, 1.11 mmol) was added to a solution of $(Et_4N)[FeCl_4]$ (0.50 g, 1.53 mmol) in 4 mL of acetonitrile. The black solution was stirred for 30 s and allowed to stand for 12−15 h during which black crystals precipitated. The crystals were collected, washed with successive aliquots of THF (3 × 5 mL) and ether (2 × 5 mL), and dried in vacuo to afford 0.089 g (37%) of product. Absorption spectrum (acetonitrile): λ_{max} (ϵ_M) 250 (sh, 63000) nm. Anal. Calcd for $C_{40}H_{100}Cl_{12}Fe_{10}N_{13}$: C, 27.49; H, 5.77; Cl, 24.35; Fe, 31.96, N, 10.42. Found: C, 27.15; H, 5.65; Cl, 24.06; Fe, 31.78; N, 10.24.

$(Et_4N)_5[Fe_{10}N_8Br_{12}]$. Neat $(Me_3Sn)_3N$ (0.34 g, 0.68 mmol) was added to a solution of $(Et_4N)[FeBr_4]$ (0.25 g, 0.50 mmol) in 3 mL of acetonitrile, causing a color change from dark orange to green-black. The reaction mixture was allowed to stand for 12−15 h, during which black, rectangular plate-shaped crystals deposited. The crystals were collected, washed with successive aliquots of THF (3 × 5 mL) and ether (3 × 5 mL), and dried in vacuo to yield 0.043 g (35%) of product. Absorption spectrum (acetonitrile): λ_{max} (ϵ_M) 300 (58000) nm.

Physical Measurements. Mössbauer spectra were recorded on two spectrometers using Janis Research Supervaritemp dewars that allowed studies in applied magnetic fields up to 8.0 T in the temperature range from 1.5 to 298 K. Spectral simulations were performed using the WMOSS software package (WEB Research, Inc., Edina, MN). Isomer shifts are quoted relative to iron metal at 298 K. EPR spectra were recorded on a Bruker EPR 300 spectrometer equipped with an Oxford ESR 910 liquid-helium cryostat and an Oxford temperature controller. Absorption spectra were measured with a Cary Bio 50 spectrophotometer.

DFT Calculations. Density functional calculations were performed with Gaussian 2003 (revision C.02)[43] using the functional B3LYP and basis set 6-311G. The structure used for the calculations of exchange coupling constants (J_{ij} between iron atoms i and j), isomer shifts (δ), and quadrupole splittings (ΔE_Q) was obtained by geometry optimization of the C_{2h} symmetrized structure of $[Fe_4N_2Cl_{10}]^{4-}$ in which the Fe-(2,2′)Cl_3 moieties are in the staggered conformation and the two-fold axis is perpendicular to the Fe_4 plane (Figure 3). For computational convenience the geometry optimization was performed for the state in which the spins of the four iron atoms are aligned ferromagnetically. The J_{ij} values were calculated in diiron systems by replacing two Fe^{3+} ions in the geometry-optimized structure with two Ga^{3+} ions. The J_{ij} values (using the convention $J_{ij}\mathbf{S}_i\cdot\mathbf{S}_j$) were obtained by the expression $J = (E(F) - E(BS)/12.5$.[44] The energies (E) for the ferromagnetic (F) and broken-symmetry (BS) states were obtained by single-point calculations, using tight convergence criteria. The DFT calculations for the ferromagnetic state (spin multiplicity parameter = 11) were conventional and used the default guess. To obtain BS solutions, we initiated SCF procedures with carefully prepared guess wave functions, in which five α electrons were assigned to 3d-type orbitals localized at Fe(i) and five β electrons to 3d-type orbitals localized at Fe(j); the remaining electrons were kept in the original default guess orbitals. The total number of α electrons was taken equal to the total number of β electrons by setting the spin multiplicity parameter equal to 1. The spin-unrestricted version, UB3LYP, of the adopted functional was used. The Nosymm option of the SCF keyword was activated to enable breaking of the orbital symmetry. The localized 3d-type orbitals for the BS calculations were constructed by performing unitary localization transformations on default guess orbitals of intermetal, $d(i)-d(j)$ type. The localization of the resulting orbitals was verified graphically with GaussView, the visualization software of Gaussian, Inc. The Mulliken spin populations are typically +4.0 (Fe(i)), +4.0 (Fe(j)) for the F solutions and +4.0 (Fe(i)), −4.0 (Fe(j)) for the BS solutions, the sign flip being the hallmark of BS. The ideal spin populations for high-spin Fe^{3+} dimers are ±5; the deficit in the computed values is due to spin delocalization toward the ligands. Isomer shifts were evaluated from the electron densities at the iron nuclei, using the calibration of Vrajmasu et al.[6] The quadrupole splittings were calculated from the DFT values for the principal components of the electric field gradient ($-V_{xx}$, $-V_{yy}$, $-V_{zz}$) at the iron nuclei using the expression $\Delta E_Q = {}^1/_2eQ(1 + \eta^2/3)^{1/2}V_{zz}$, the convention $|V_{xx}| \le |V_{yy}| \le |V_{zz}|$, and the nuclear quadrupole moment $Q(^{57}Fe) = 0.16$ barn.

X-ray Structure Determinations. Structures of the five compounds in Table 1 have been determined. Suitable crystals of $(Et_4N)_4[Fe_4N_2X_{10}]$ (X = Cl^-, Br^-) and $(Et_4N)_4[Fe_4N_2Cl_{10}]$·2MeCN were obtained by addition of THF to the reaction mixture in acetonitrile. The solvated and unsolvated salts of $[Fe_4N_2Cl_{10}]^{4-}$ cannot be reliably distinguished by morphology. Crystals of $(Et_4N)_5[Fe_{10}N_8Cl_{12}]$·2MeCN and $(Et_4N)_5$-$[Fe_{10}N_8Br_{12}]$ grew directly from the reaction mixtures. Crystals were coated with paratone-N oil and mounted on a Bruker SMART CCD diffractometer which was operated at 193 K. Initial lattice parameters were obtained from a least-squares analysis of more than 50 carefully centered reflections using SMART software; these parameters were subsequently refined against all data using SAINT. None of the crystals showed significant decay during data collection. Absorption corrections were applied using SADABS. Space group assignments were based on systematic absences, E-statistics, and successful refinement of the structures. Structures were solved by direct methods with the aid of successive difference Fourier maps and were refined against all data using the SHELXTL 5.0 package. Thermal parameters for all non-

(43) Frisch, M. J.; Trucks, G. W.; Schlegel, H. B.; Scuseria, G. E.; Robb, M. A.; Cheeseman, J. R.; Montgomery, J. A., Jr.; Vreven, T.; Kudin, K. N.; Burant, J. C. et al. *Gaussian 03*; Gaussian, Inc., Wallingford, CT, 2004.
(44) Noodleman, L.; Baerends, E. J. *J. Am. Chem. Soc.* **1984**, *106*, 2316−2327.

hydrogen atoms were refined anisotropically. Hydrogen atoms were placed at idealized positions and were refined isotropically. Three of the five cations in the crystal structure of $(Et_4N)_5[Fe_{10}N_8Br_{12}]$ gave evidence of disorder and were modeled accordingly; thermal parameters of the disordered carbon and nitrogen atoms were refined anisotropically. Crystal parameters and final agreement factors are contained in Table 1.[45] Also isolated were black platelike crystals of $(Et_4N)_4[Fe_4N_2Cl_{10}]$ in triclinic space group $P\bar{1}$ with $a = 11.278$ Å, $b = 11.609(4)$ Å, $c = 11.952(4)$ Å, $\alpha = 107.71(3)°$, $\beta = 103.56(2)°$, and $\gamma = 107.50(2)°$. The structure of the cluster was the same as that in the monoclinic form.

In the sections that follow, clusters are designated **1**−**4** as in Table 1.

Results and Discussion

Synthesis of Clusters. In the synthesis of metal-nitride complexes, sources of nitride include NH_3, N_3^-, NO, and much less frequently, $(Me_3Si)_3N$.[46,47] In seeking other nitride-transfer reagents more suitable for the goal at hand, the compounds $(Me_3E)_3N$ (E = Si, Ge, Sn) were particularly attractive. One example of their utility is the reaction of $(Me_3Si)_3N$ with WCl_6 to form $[W_2(\mu_2\text{-}N)Cl_9]$ or $[WNCl_3]$ and Me_3SiCl.[48] Given the bond dissociation energy trend Si−X > Ge−X > Sn−X at constant X,[49−51] and the bond energy differences [Si−N] − [Sn−N] ≈ 15−20 kcal/mol, stannylamines are potentially more reactive as nitride sources. We were cognizant of the reported cleavage of Sn−N bonds of $(Me_3Sn)_3N$ and other stannylamines by metal-halide complexes,[48,52−56] with formation of molecular metal nitrides in several cases. Accordingly, $(Me_3Sn)_3N$ was employed in this investigation as the nitride-transfer reagent.

The synthetic schemes leading to two molecular iron nitrides are depicted in Figure 2; clusters were isolated as black Et_4N^+ salts. The compound $(Me_3Sn)_3N$ undergoes a rapid reaction with $[FeCl_4]^{1-}$ when combined in a 2:1 mol ratio in acetonitrile solution. The initial light yellow solution immediately changes to black. When the reaction is monitored by ^1H NMR, all the stannylamine is consumed after about 15 min, and at the completion of the reaction the only tin-containing product detected is Me_3SnCl. Reaction 1 describes the formation of tetranuclear Fe^{III} cluster **1**, obtained in 72% yield.

$$4[FeCl_4]^{1-} + 2(Me_3Sn)_3N \rightarrow [Fe_4N_2Cl_{10}]^{4-} + 6Me_3SnCl \quad (1)$$

Further clusters were sought by varying the mol ratio of the reactants. After some experimentation, an 11:8 ratio was found to afford the decanuclear cluster **3** as the mixed-valence ($9Fe^{III}$ + Fe^{IV}) penta-anion. Reaction 2 is suggested as the overall stoichiometry for the formation of **3**, isolated in 37% yield.

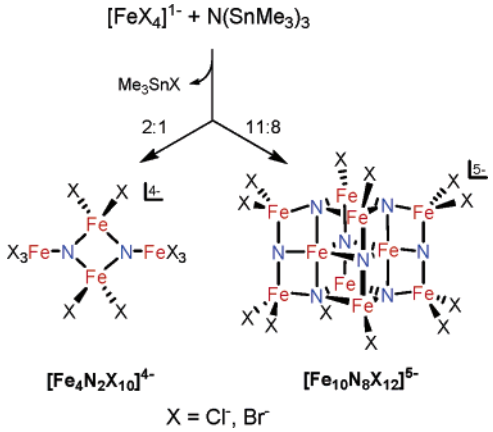

Figure 2. Synthesis of the clusters $[Fe_4N_2X_{10}]^{4-}$ and $[Fe_{10}N_8X_{12}]^{5-}$ (X = Cl^-, Br^-). The molar ratios $[FeX_4]^{1-}$:$N(SnMe_3)_3$ are indicated.

$$11[FeCl_4]^{1-} + 8(Me_3Sn)_3N \rightarrow [Fe_{10}N_8Cl_{12}]^{5-} + 24Me_3SnCl + [FeCl_4]^{2-} + 4Cl^- \quad (2)$$

A possible scenario is initial formation of $[Fe_{10}N_8Cl_{12}]^{6-}$ followed by one-electron oxidation to **3**. The two clusters can be distinguished by their UV−visible spectra (Experimental Section), and both obey Beer's law in acetonitrile. In solution, these clusters are extremely sensitive to trace amounts of water. Based on absorption spectra, cluster **1** remains intact in acetonitrile after 24 h. Decomposition does not exceed ∼1% in 24 h; after 72 h, ∼75% of the cluster remained.

Bromide clusters **2** (58%) and **4** (35%), isostructural with **1** and **3**, respectively, were prepared by analogous methods. They appear to be less stable in solution than the chloride clusters and apparently decompose through a redox process. Crystals of $(Et_4N)_2[FeBr_4]$, identified by isomorphism with $(Et_4N)_2[MnBr_4]$,[57] were isolated from a solution of **2** in acetonitrile for 24 h, together with an unidentified black powder, upon introduction of ether or THF by vapor diffusion.

Cluster Structures. The structures of the Et_4N^+ salts of clusters **1**−**4** have been determined. Structures of **1** and **3** are shown in Figures 3 and 4, respectively. Selected metric data are collected in Tables 2 and 3. Discussion is limited to the chloride clusters; their bromide analogues **2** and **4** are isostructural with near isometric cores.

(a) $[Fe_4N_2Cl_{10}]^{4-}$. The dimensions of cluster **1** are nearly identical in the solvated and unsolvated crystals, and centrosymmetry is imposed in both. Metric data (Table 2) refer to the unsolvated form. The $[Fe^{III}{}_4N_2]^{6+}$ core contains an $Fe^{III}{}_2(\mu_3\text{-}N)_2$ core rhombus with Fe−N = 1.879(2) Å, Fe···Fe = 2.6110(6) Å, N−Fe−N = 91.95(6)°, and Fe−N−Fe = 88.05(6)°. Each iron atom is terminally coordinated by two chlorides, and each nitrogen atom is bonded by one $FeCl_3$ unit (Figure 3). The Fe_4N_2 core closely approaches planarity. Small displacements of N and Fe atoms from the Fe1N1Fe2 (0.05 Å) and rhombus (0.12 Å) planes, respectively, impart a distorted trigonal plane geometry to the nitrogen atoms. The iron sites display distorted tetrahedral stereochemistry with the principal distortion being

(45) See paragraph at the end of this article for Supporting Information available.
(46) Dehnicke, K.; Strähle, J. *Angew. Chem., Int. Ed. Engl.* **1981**, *20*, 413−426.
(47) Dehnicke, K.; Strähle, J. *Angew. Chem., Int. Ed. Engl.* **1992**, *31*, 955−978.
(48) Godemeyer, T.; Berg, A.; Gross, H.-D.; Müller, U.; Dehnicke, K. *Z. Naturforsch.* **1985**, *40b*, 999−1004.
(49) Leroy, G.; Temsamani, D. R.; Wilante, C. *J. Mol. Struct. (THEOCHEM)* **1994**, *306*, 21−39.
(50) Basch, H. *Inorg. Chim. Acta* **1996**, *252*, 265−279.
(51) Luo, Y.-R. *Handbook of Bond Dissociation Energies in Organic Compounds*; CRC Press: New York, 2003; pp 287−299.
(52) Dilworth, J. R.; Hanich, J.; Krestel, M.; Beck, J.; Strähle, J. *J. Organomet. Chem.* **1986**, *315*, C9−C12.
(53) Plenio, H.; Roesky, H. W.; Noltemeyer, M.; Sheldrick, G. M. *Angew. Chem., Int. Ed. Engl.* **1988**, *27*, 1330−1331.
(54) Bai, Y.; Roesky, H. W.; Schmidt, H.-G.; Noltemeyer, M. *Z. Naturforsch.* **1992**, *47b*, 603−608.
(55) Decker, A.; Fenske, D.; Maczek, K. *Angew. Chem., Int. Ed. Engl.* **1996**, *35*, 2863−2866.
(56) Reiss, P.; Fenske, D. *Z. Anorg. Allg. Chem.* **2000**, *626*, 1317−1331.
(57) Cotton, F. A.; Daniels, L. M.; Huang, P. *Inorg. Chem.* **2001**, *40*, 3576−3578.

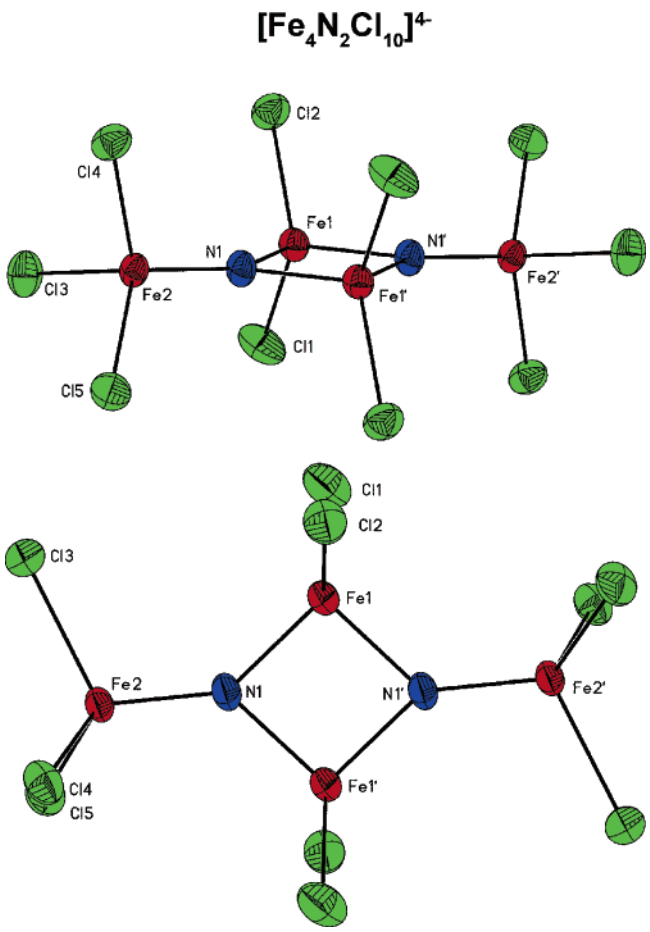

Figure 3. Structure of $[Fe_4N_2Cl_{10}]^{4-}$ from the side (upper) and down the idealized C_2 axis (lower) showing 50% probability ellipsoids and the atom-labeling scheme. Primed and unprimed atoms are related by a crystallographic inversion center. $[Fe_4N_2Br_{10}]^{4-}$ is isostructural (not shown).

the restricted N−Fe−N angle of the rhombus (*ca*. 92°). The Fe_4N_2 portion of the cluster approaches idealized D_{2h} symmetry. However, the displacements of Fe(2,2′) above and below the rhombus plane lowers the symmetry to C_{2h}, and the inequivalence of the angles Fe2−N1−Fe1/Fe1′ further reduces the symmetry to C_i. As viewed down the Fe2−N1−N1′−Fe2′ vector, the chloride ligands are in a staggered conformation. The Fe−Cl distances in **1** (2.24−2.27 Å) are longer than in $[FeCl_4]^{1-}$ (2.182 Å).[58] This expansion is confirmed by DFT geometry optimizations for these systems and may be due to the large negative charge of the cluster.

In the context of related structures and structural features, we note the two previous examples of trigonal planar nitride, found in $[Cp_3Mo_3O(\mu_3\text{-}N)(SMe)_4]$[59] and the classic Delépine complex $[Ir_3(\mu_3\text{-}N)(SO_4)_6(OH_2)_3]^{4-}$.[60] The only other cluster to contain the planar $[M_4N_2]^{6+}$ core is $[Cp^*_4Al_4(\mu_3\text{-}N)_2(N(SiMe_3)_2)_2]$.[61] Planar and nonplanar $[Fe_4(\mu_3\text{-}O)_2]^{8+}$ cores are found in a variety of complexes[62−64] and present an atom connectivity analogous to that of **1** and **2**.

Table 2. Selected Interatomic Distances (Å) and Angles (deg) of the $[Fe_4N_2X_{10}]^{4-}$ (X = Cl, Br) Anion

	$(Et_4N)_4$[**1**]	$(Et_4N)_4$[**1**]·2MeCN	$(Et_4N)_4$[**2**]
Fe1−N[a]	1.879(2)	1.88(1)	1.874(2)
Fe2−N	1.755(2)	1.758(2)	1.753(2)
Fe1−Fe1′	2.6110(6)	2.624(1)	2.6088(9)
N1−Fe−N1′	91.95(6)	91.65(8)	91.86(9)
Fe1−N1−Fe1′	88.05(6)	88.35(8)	88.14(9)
Fe2−N1−Fe1	140.62(9)	139.1(1)	135.8(1)
Fe2−N1−Fe1′	131.06(8)	132.0(1)	134.7(1)
Fe1−X[a]	2.2434(2)	2.2594(7)	2.393(6)
Fe2−X[a]	2.274(5)	2.268(9)	2.411(6)
X−Fe1−N	112.65(5)−116.67(5)	112.90(6)−116.04(6)	113.69(7)−114.77(8)
	114(2)[a]	114(1)[a]	114.1(4)[a]
X−Fe2−N	110.82(6)−113.89(5)	110.45(6)−112.86(6)	108.53(8)−114.53(7)
	112(2)[a]	111(1)[a]	111(3)[a]
X−Fe1−X	108.48(2)	107.18(4)	107.92(2)
X−Fe2−X	105.30(2)−107.75(2)	106.06(4)−109.45(3)	106.45(2)−109.58(2)
	107(1)[a]	107(2)[a]	108(2)[a]
Fe2−X[b]	110	77	74
$d_\perp$(N1)[c]	−0.052	0.075	−0.12
$d_\perp$(Fe2)[d]	0.12	0.17	0.27

[a] Mean values. [b] Dihedral angle between the [Fe1,N1,Fe1′] rhombic plane and the [X,Fe2,Fe2′] least-squares fitted plane which approaches perpendicular. [c] Perpendicular displacement of N1 from [Fe1,Fe2,Fe1′] plane. [d] Perpendicular displacement of Fe2 from the Fe_2N_2 plane. Symmetry equivalents are denoted by primed atoms.

(b) $[Fe_{10}N_8Cl_{12}]^{5-}$. The composition and structure of cluster **3** lead to the mixed-valence core formulation $[Fe^{III}_9Fe^{IV}(\mu_3\text{-}N)_2(\mu_4\text{-}N)_6]^{7+}$. Cluster **3** has no crystallographically imposed symmetry but approaches idealized D_{2h} symmetry (Figure 4), in which case six core atoms (e.g., in the set Fe1Fe2Fe5N1N3N4) are unique. Inspection of the structure reveals three types of nitride-bridging interactions. Atoms N(3,6) bridge in a T-shape (μ_3-N_T), N(1,2,7,8) assume trigonal pyramidal bridge stereochemistry (μ_4-N_{tp}), and N(4,5) adopt a butterfly arrangement (μ_4-N_{bf}). To provide an economical description, bond distances are averaged, and bond angles are collected under this symmetry (Table 3), which represents a good approximation except for four angles in the N3−Fe5−N4 set. These and other structural elements are referred to by a member of a symmetrically equivalent set. The structure consists of 15 fused Fe_2N_2 distorted rhomboids (hereafter, for simplicity, rhomboids). Four rhomboids (Fe1N1Fe5N3) share two edges each at the exterior of the structure. The iron atoms occur in Fe(μ_3-N_T)(μ_4-N_{tp})Cl_2 distorted tetrahedral sites. These rhomboids are conjoined by the two μ_3-N_T atoms and Fe5 and Fe6, which possess distorted trigonal bipyramidal Fe(μ_3-N_T)(μ_4-N_{tp})$_2$(μ_4-N_{bf})$_2$ coordination. Eight interior rhomboids (Fe2N1Fe5N4) share three edges each. These can be visualized as two distorted cubes sharing a common rhomboidal face (Fe5Fe6N4N5) in which all edges are shared. The top (Fe2N1Fe3N2) and bottom faces of the dicube portion are rhomboids in which the iron atoms are in distorted tetrahedral Fe(μ_4-N_{tp})$_2$(μ_4-N_{bf})Cl sites. Cluster **3** can be visualized as an $[Fe_2N_4]^{5-}$ entity sandwiched by two neutral $[Fe_4N_2Cl_6]$ units, derived from **1** by removal of four chloride ligands.

The data of Table 3 reveal that all rhomboids have comparable mean dimensions, with Fe−N−Fe < 90° and N−Fe−N ≳ 90°. Individual Fe−N bond lengths occur in the interval 1.81−2.04 Å. There is no clear indication from bond lengths of a discrete Fe^{IV} site. The exterior rhomboids have the shorter Fe−N distances (e.g., Fe1−N3 = 1.823(7) Å), resulting in the four

(58) Cotton, F. A.; Murillo, C. A. *Inorg. Chem.* **1975**, *14*, 2467−2469.
(59) Shollhammer, P.; Pétillon, F. Y.; Talarmin, J.; Muir, K. W. *J. Organomet. Chem.* **1998**, *560*, 245−251.
(60) Ciechanowicz, M.; Griffith, W. P.; Pawson, D.; Skapski, A. C. *Chem. Commun.* **1971**, 876.
(61) Schulz, S.; Häming, L.; Herbst-Irmer, R.; Roesky, H. W.; Sheldrick, G. M. *Angew. Chem., Int. Ed.* **1994**, *33*, 969−970.
(62) Armstrong, W. H.; Roth, M. E.; Lippard, S. J. *J. Am. Chem. Soc.* **1987**, *109*, 6318−6326.
(63) Gorun, S. M.; Lippard, S. J. *Inorg. Chem.* **1988**, *27*, 149−156.
(64) Çelenligil-Çetin, R.; Staples, R. J.; Stavropoulos, P. *Inorg. Chem.* **2000**, *39*, 5838−5846.

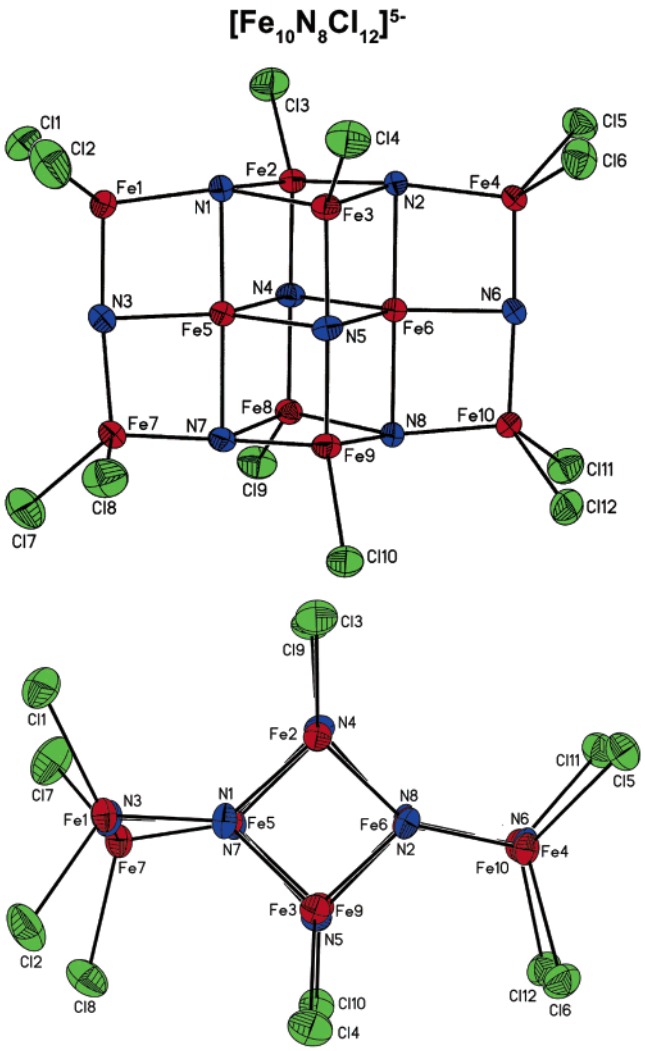

Figure 4. Structure of $[Fe_{10}N_8Cl_{12}]^{5-}$ from the side (upper) and down the idealized C_2 axis (lower) showing 50% probability ellipsoids at the atom-labeling scheme. $[Fe_{10}N_8Br_{12}]^{5-}$ is isostructural (not shown).

μ_4-N_{tp} atoms lying above (N1) or below (N7) the Fe_3 plane of bonded atoms by 0.16−0.17 Å. The planes Fe2Fe3N1N2 and Fe5Fe6N4N5 are essentially perfect (atom deviations <0.07 Å) and parallel (dihedral angles 0.5°, 0.7°), as is the plane Fe1Fe4Fe7Fe10 (0.11−0.12 Å) containing the four terminal iron atoms of the cluster and the plane N1N2Fe5Fe6N7N8 (≤0.04 Å) locating six interior atoms of the dicube portion. The interior atoms Fe5 and Fe6 reside in distorted trigonal bipyramidal sites, as indicated by the parameters for Fe5, especially the nearly linear N1−Fe5−N7 arrangement. Because of angular deformations and the short Fe(5)−N_3 interaction of 1.915(4) Å compared to the mean of 2.02(2) Å for the other four bonds, the site symmetry of Fe(5) is C_{2v} rather than D_{3h}. As would be expected, the dimensions of the Fe_2N_2 rhomboids compare rather closely with those of the imido-ligated cores of $[Fe_2(\mu_2\text{-NR})_2Cl_4]^{2-}$ and the faces of the cubanes $[Fe_4(\mu_3\text{-NR})_4Cl_4]^{2-,1-,0}$.[39,40]

In all iron *molecular* nitride clusters, there is no reported occurrence of a μ_3-N or a μ_4-N_{tp} atom. The μ_4-N_{bf} bridging mode has been established in $[Fe_4N(CO)_{12}]^{1-}$ and its substitution products.[29,32,65,66] The μ_6-N structural element, of prime interest because of its presence in FeMoco,[1] was not encountered in this work. Its occurrence in synthetic iron species is thus far confined to the low-valent carbonyl cluster $[Fe_6N(CO)_{15}]^{2-}$ and several of its derivatives.[32,67] If the scope is expanded to the solid state, μ_6-N bridges are found in phases such as ϵ-Fe_3N and γ'-Fe_4N.[68]

Electronic Properties. To probe their ground-state features, clusters **1** and **3** have been examined by Mössbauer spectroscopy and **3** by EPR spectroscopy. Spectra are shown in Figures 5−7; Mössbauer parameters are collected in Table 4. In addition, DFT calculations have been performed on **1** to ascertain the major exchange pathways.

(a) $[Fe_4N_2Cl_{10}]^{4-}$. Mössbauer spectra recorded in zero magnetic field and in a magnetic field of 8.0 T applied parallel to the γ-ray beam are shown in Figure 5. The spectrum of Figure 5A consists of two nested quadrupole doublets whose isomer shifts are in the range commonly observed for high-spin (S_i = $^5/_2$) Fe^{III}. The observation that the iron sites are equivalent in pairs is in accord with the X-ray structure. The 8.0 T spectra recorded at 4.2, 77, 100, and 160 K were essentially identical. The features of the 4.2 K spectrum (not shown) can be fitted well by assuming that the cluster spin of the ground state is S = 0. Close inspection of the data shows that the sample contains an unknown contaminant accounting for ca. 5% of the total iron.

From the observation that the 77, 100, and 160 K high-field spectra can be well simulated for S = 0, we infer a lower limit for the dominant exchange coupling constant based on the following arguments. The idealized D_{2h} symmetry of the Fe_4N_2 portion suggests that the exchange coupling can be described by three coupling constants. Using the numbering scheme below, these are J ($J = J_{13} = J_{14} = J_{23} = J_{24}$), J_{12}, and J_{34}. Consequently, we apply the exchange Hamiltonian in eq 3 with $S_1 = S_2 = S_3 = S_4 = {}^5/_2$. Coupling $\mathbf{S}_1 + \mathbf{S}_2 = \mathbf{S}_{12}$, $\mathbf{S}_3 + \mathbf{S}_4 =$

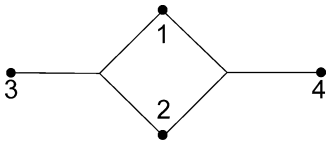

$\mathbf{S}_{34}$, $\mathbf{S}_{12} + \mathbf{S}_{34} = \mathbf{S}$ with the restrictions $0 \le S_{12} \le 5$, $0 \le S_{34} \le 5$, and $|S_{12} - S_{34}| \le S \le S_{12} + S_{34}$ yields the energies e of eq 4 where the constant terms $JS_i(S_i + 1)$ ($S_i = {}^5/_2$, i = 1,4) that affect all levels have been dropped.

$$H_{ex} = J(\mathbf{S}_1\cdot\mathbf{S}_3 + \mathbf{S}_1\cdot\mathbf{S}_4 + \mathbf{S}_2\cdot\mathbf{S}_3 + \mathbf{S}_2\cdot\mathbf{S}_4) + J_{12}\mathbf{S}_1\cdot\mathbf{S}_2 + J_{34}\mathbf{S}_3\cdot\mathbf{S}_4 \quad (3)$$

$$\epsilon(S,S_{12},S_{34}) = {}^1/_2\{JS(S+1) + (J_{12} - J)S_{12}(S_{12}+1) + (J_{34} - J)S_{34}(S_{34}+1)\} \quad (4)$$

To estimate the exchange coupling constants J, J_{12}, and J_{34}, we have performed DFT calculations using the broken symmetry approach.[44,69,70] We have simplified the computational problem by substituting two Ga^{3+} for two Fe^{3+}. By placing Ga^{3+} into

(65) Gourdon, A.; Jeannin, Y. *J. Organomet. Chem.* **1992**, *440*, 353−366.
(66) Zanello, P.; Laschi, F.; Cinquantini, A.; Della Pergola, R.; Garlaschelli, L.; Cucco, M.; Demartin, F.; Spalding, T. R. *Inorg. Chim. Acta* **1994**, *226*, 1−8.
(67) Della Pergola, R.; Garlaschelli, L.; Manassero, M.; Sansoni, M.; Strumolo, D.; Fabrizi de Biani, F.; Zanello, P. *J. Chem. Soc., Dalton Trans.* **2001**, 2179−2183.
(68) Jacobs, H.; Rechenbach, D.; Zachwieja, U. *J. Alloys Cmpds.* **1995**, *227*, 10−17.
(69) Noodleman, L. *J. Chem. Phys.* **1981**, *74*, 5737−5743.
(70) Rodriguez, J. H.; McCusker, J. K. *J. Chem. Phys.* **2002**, *116*, 6253−6270.

Table 3. Bond Distances (Å) and Angles (deg) of $[Fe_{10}N_8Cl_{12}]^{5-}$ under Idealized D_{2h} Symmetry

distance/angle[a]	n[b]	mean/range	distance/angle[a]	n[b]	mean/range
	μ_3-N_T(3,6)[c]			**Fe(1−10)**	
Fe1−N3	4	1.823(7)	Fe1−Cl1	8	2.26(2)
Fe5−N3	2	1.91(1)	Fe2−Cl3	4	2.216(5)
Fe1−N3−Fe5	4	87.7(2)−88.9(2)	Fe1−Fe5	4	2.600(9)
Fe1−N3−Fe7	2	169.3(3), 176.8(2)	Fe2−Fe3	2	2.68(3)
	μ_4-N_{tp}(1,2,7,8)[d]		Fe2−Fe5	8	2.69(3)
Fe1−N1	4	1.87(2)	Fe5−Fe6	1	2.757(1)
Fe2−N1	8	1.934(9)	N1−Fe1−N3	4	97.0(2)−97.5(2)
Fe5−N1	4	2.01(1)	N1−Fe2−N2	4	91.0(2)−93.3(1)
Fe1−N1−Fe2	8	122.2(2)−147.3(2)	N1−Fe5−N3	4	89.4(2)−90.6(1)
Fe1−N1−Fe5	4	84.2(1)−87.2(2)	N3−Fe5−N4	4	124.9(2)−140.7(2)
Fe2−N1−Fe3	4	86.6(2)−88.3(2)	N4−Fe5−N5	2	94.1(2), 94.3(2)
	μ_4-N_{bf}(4,5)[e]		N1−Fe5−N4	8	88.8(2)−91.5(1)
Fe2−N4	4	1.89(1)	N1−Fe5−N7	2	176.5(2), 178.6(2)
Fe5−N4	4	2.03(2)	N1−Fe1−Cl1	8	106.8(1)−115.7(1)
Fe2−N4−Fe5	8	85.7(2)−87.9(2)	N1−Fe2−Cl3	8	117.1(1)−128.2(1)
Fe5−N4−Fe6	2	85.7(2), 86.3(2)	Cl1−Fe1−Cl2	4	105.87(6)−112.22(7)
Fe2−N4−Fe8	2	170.9(3), 171.1(3)			

[a] Type included in average or range; other members of the set are symmetry-related. [b] Number in the set. [c] T, T-shaped. [d] tp, trigonal pyramidal. [e] bf, butterfly.

Table 4. Mössbauer Parameters of Clusters 1 and 3

	site	δ (mm/s)	ΔE_Q (mm/s)	η[a]
$[Fe_4N_2Cl_{10}]^{4-}$[b]	$FeNCl_3$	0.42(1)	−2.24(3)	0.3(2)
	FeN_2Cl_2	0.41(1)	+1.08(2)	0.6(3)
$[Fe_{10}N_8Cl_{12}]^{5-}$[c]	FeN_2Cl_2	0.35(1)	1.08(2)[e]	—[e]
	FeN_3Cl[d]	0.36	0.64[e]	[e]
	FeN_5[d]	0.32	0.34[e]	[e]

[a] $\eta = (V_{xx} - V_{yy})/V_{zz}$. [b] 4.2 K. [c] 150 K. [d] Provisional values; see text. [e] η and the sign of ΔE_Q have not been determined.

sites 2 and 4, sites 3 and 4, and sites 1 and 2, exchange pathways linking sites 1 and 3, sites 1 and 2, and sites 3 and 4, respectively, are isolated. Because of nearly identical tetrahedral ionic radii (Fe^{3+} 0.63 Å, Ga^{3+} 0.61 Å),[71] Ga^{3+} is known to substitute isomorphously for high-spin Fe^{3+}.[72] While such substitution will have some effect on the exchange pathways to be evaluated, we expect that they will impose no major perturbations. The DFT results show that the changes in the Mulliken charges of the critical Fe^{3+} and nitrido sites, for which the exchange pathway is evaluated, are small (<0.1 e^-). Using the same geometry-optimized structure[73] for the three cases, we obtained the antiferromagnetic coupling constants $J = 261$ cm^{-1}, $J_{12} = 140$ cm^{-1}, and $J_{34} = 29$ cm^{-1}. Although the accuracy of these calculations is difficult to assess in the absence of suitable experimental data, the results suggest that the exchange pathway described by J is dominant.

With the information obtained by DFT calculations, it follows from eq 4 that the diamagnetic $|S, S_{12}, S_{34}, M_S\rangle = |0, 5, 5, 0\rangle$ state is the ground state and that the first excited spin multiplet $|1, 5, 5, M\rangle$ has energy J. The magnetic hyperfine interactions of the four high-spin ferric ions are expected to be isotropic and described by $A_i\mathbf{S}_i\cdot\mathbf{I}_i$, with $A_1 = A_2$ and $A_3 = A_4$. When the electronic system is in the first excited state $|1, 5, 5, M\rangle$, these terms can be expressed as $A_i\mathbf{S}\cdot\mathbf{I}_i$ with the system spin $S = 1$.[74]

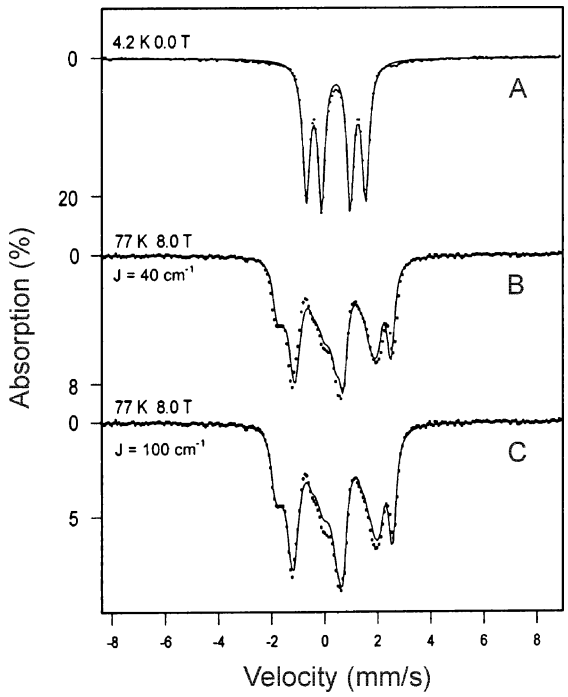

Figure 5. Mössbauer spectra of polycrystalline $(Et_4N)_4[Fe_4N_2Cl_{10}]$ recorded (A) in zero field at 4.2 K and (B,C) at 77 K in an applied field of 8.0 T. The solid line in (A) is a least-squares fit to two nested doublets yielding the parameters in Table 4. The solid line in (B) is a spectral simulation obtained by assuming fast relaxation of the electron spin and $J = 40$ cm^{-1}. The theoretical curve in (C) was obtained by assuming $J = 100$ cm^{-1}. A J-value of 100 cm^{-1} produces at 77 K a vanishingly small internal magnetic field at the nucleus, and the simulation is essentially indistinguishable from that obtained for diamagnetic sites.

Typical A-values of high-spin ferric sites are $A_i = -(27$ to $29)$ MHz, and we have used $A_i = -28$ MHz to establish a lower limit for J from the analysis of the 8.0 T, 100 K spectrum. The methodology of determining J from spectra of spin-coupled clusters with a diamagnetic ground state has been described previously.[75,76]

(71) Shannon, R. D. *Acta Crystallogr.* **1976**, *A32*, 751−767.
(72) Maelia, L. E.; Koch, S. A. *Inorg. Chem.* **1986**, *25*, 1896−1904.
(73) This structure was obtained by geometry optimization of the idealized C_{2h} structure. The optimization was performed for the state in which the spins of the four iron atoms are aligned ferromagnetically. In our experience, spin ordering has only a minor influence of metal−ligand distance.
(74) The calculation of the Mössbauer spectra in the present case is equivalent to calculating spectra for an antiferromagnetically coupled $Fe^{3+}Fe^{3+}$ cluster described by $H_{exch} = J\mathbf{S}_1\cdot\mathbf{S}_2$ with $S_1 = S_2 = 5/2$, and using for the intrinsic A-values half the magnitude of typical high-spin ferric sites.
(75) Kauffmann, K.; Münck, E. In *Spectroscopic Methods in Bioinorganic Chemistry*; Solomon, E. I., Hodgson, K. O., Eds.; ACS Symposium Series 692; American Chemical Society: Washington, DC, 1998; pp 16−29.
(76) Krebs, C.; Bollinger, J. M., Jr.; Theil, E. C.; Huynh, B. H. *J. Biol. Inorg. Chem.* **2002**, *7*, 863−869.

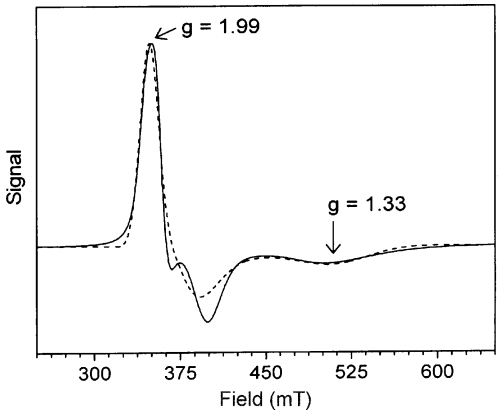

Figure 6. X-band EPR spectrum of polycrystalline $(Et_4N)_5[Fe_{10}N_8Cl_{12}]$ recorded at 2.2 K with 10 mT modulation at 100 kHz and 200 μW microwave power. The dashed line is a spectral simulation for $g_{max} = 1.99$, $g_{mid} = 1.83$, and $g_{min} = 1.33$. To account for the broadness of the lines, the g-values were distributed on a Gaussian with $\sigma_{max} = 0.0896$.

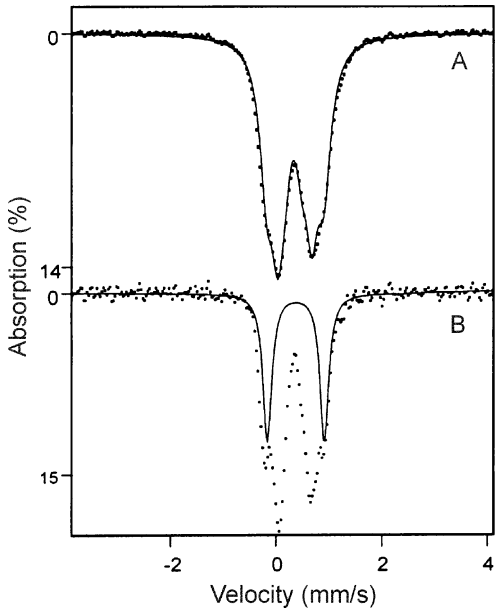

Figure 7. Mössbauer spectrum of polycrystalline $(Et_4N)_5[Fe_{10}N_4Cl_{12}]$ recorded at 150 K in zero field (A). The spectrum shown in (B) was obtained by removing the line width contribution of the ^{57}Co(Rh) source by a Fourier transform procedure. The solid line in (B) outlines the doublet of the FeN_2Cl_2 sites. The solid line in (A) is the result of a least-squares fit obtained by assuming three doublets with a 4:4:2 area ratio, keeping ΔE_Q and δ of the FeN_2Cl_2 sites fixed to the values in (B).

To provide an indication of the sensitivity of the method, we consider the 77 K spectrum of Figure 5B and C and show in Figure 5B a theoretical spectrum (solid line) for $J = 40$ cm^{-1}. It can be seen that the calculated splittings are too small, implying that the assumed population of the $S = 1$ multiplet is too high. Correct splittings are obtained for $J \geq 90$ cm^{-1} (Figure 5C); for $J \geq 90$ cm^{-1}, the spectra are essentially independent of J and identical to those of a diamagnet. The DFT value is consistent with the empirical inequality.[77]

DFT calculations for geometry-optimized cluster **1** using the C_{2h} symmetric, staggered conformation with the two-fold axis perpendicular to the Fe_4 rhomb and ferromagnetic spin alignment yield the Mössbauer parameters $\delta = 0.36$ mm/s, $\Delta E_Q = 1.38$ mm/s, and $\eta = 0.3$ for the $Fe^{III}N_2Cl_2$ site, and $\delta = 0.36$ mm/s, $\Delta E_Q = -2.91$ mm/s, and $\eta = 0.5$ for $Fe^{III}NCl_3$ site. For calculation of the isomer shift, we have used the previously established calibration[6] which, however, does not include any nitrido species. In our previous work, we had estimated that the DFT calculations should give δ values to within ± 0.04 mm/s. A large negative ΔE_Q for a spherical Fe^{3+} ion, as observed for the terminal iron atoms, indicates a sizable compilation of ligand electrons along one of the spatial directions, here along the Fe−N axis. While the calculated parameters do not closely match the experimental result (Table 4; the deviations are not atypical for DFT calculations[78,79]), they distinguish correctly between the two coordination environments of **1**. (We show below that the site with $\Delta E_Q = \pm 1.08$ mm/s corresponds to $Fe^{III}N_2Cl_2$.)

(b) $[Fe_{10}N_8Cl_{12}]^{5-}$. An X-band EPR spectrum of polycrystalline **3** at 2.2 K is shown in Figure 6. The shape of the EPR spectrum of **3** is very temperature sensitive. Below ca. 8 K the spectra exhibit passage effects, especially in the central portion of the spectra. (Decreasing our standard 100 kHz modulation to 12.5 kHz did not improve the situation.) At $T > 8$ K the spectra broadened due to increased spin relaxation. The spectrum of Figure 6 is characteristic of an $S = {}^1/_2$ ground state, with g-values at $g_{max} = 1.99$ and $g_{min} = 1.33$. The dashed line drawn through the experimental data is a spectral simulation using the parameters specified in the figure. Our simulations do not match well the minimum around 400 mT. It is possible that the sample contains a contaminant that contributes a feature around 370−380 mT, although saturation studies did not give any evidence for such a contaminant. Alternatively, a nonsimulated solid-state effect may operate. Roughly, $g_{mid} = 1.81-1.86$. It is noteworthy that the spectrum of polycrystalline **3** extends to $g \approx 1.33$. This is reminiscent of the situation in certain $Fe^{III}Fe^{II}$ clusters with local high-spin states for which zero-field splittings are comparable in magnitude with the exchange coupling constant J.[80] The "D/J mixing" shifts g-values considerably upfield. Above 10 K, the EPR spectrum broadens considerably, perhaps by Orbach spin relaxation involving low-lying spin multiplets.

The Mössbauer spectrum of polycrystalline **3** at 150 K is presented in Figure 7A. At this temperature, the electronic spin is in the fast fluctuation limit and only quadrupole doublets are observed. To increase resolution, the line width contribution of the Co^{57}(Rh) source has been removed by a Fourier transform procedure;[81] the resultant spectrum is shown in Figure 7B. At least two types of iron environments can be discerned. One type, accounting for ca. 40% of the iron, is indicated by the simulated quadrupole doublet (solid line). Its Mössbauer parameters, $\delta = 0.35$ mm/s (corresponding to $\delta \approx 0.39$ mm/s at 4.2 K after correction for the second-order Doppler shift) and $\Delta E_Q = 1.08$ mm/s closely match those for the $Fe^{III}N_2Cl_2$ sites. Since these sites are the only ones that **1** and **3** have in common, we assign these parameters to them (Table 4). Formally, cluster **3** has one Fe^{IV} site. A localized Fe^{IV} site is expected to exhibit a smaller

(77) Magnetic susceptibility measurements for J have not been attempted. This approach is problematic because the small paramagnetic magnetization of the cluster has to be evaluated in the presence of an unknown paramagnetic impurity.

(78) Neese, F. *Inorg. Chim. Acta* **2002**, *337*, 181−192.
(79) Zhang, Y.; Mao, J.; Oldfield, E. *J. Am. Chem. Soc.* **2002**, *124*, 7829−7839.
(80) Sage, J. T.; Xia, Y.-M.; Debrunner, P. G.; Keough, D. T.; de Jersey, J.; Zerner, B. *J. Am. Chem. Soc.* **1989**, *111*, 7239−7247.
(81) Dibar-Ure, M. C.; Flinn, P. A. In *Mössbauer Effect Methodology*; Gruverman, I. J., Ed.; Plenum Press: New York, 1971; pp 245−262.

isomer shift (typically −0.2 to 0.2 mm/s) than those of ferric sites. The $Fe^{IV}Fe^{IV}$ nitride-bridged dinuclear complexes (Figure 1) at 77−130 K have isomer shifts of −0.10 to 0.04 mm/s.[19−21,82] We have not been able to find a site with an isomer shift in this range. However, given the symmetry of the cluster, it is likely that delocalization occurs, perhaps over an $Fe^{III}Fe^{IV}$ pair or a $3Fe^{III}Fe^{IV}$ portion of the cluster not involving $Fe^{III}N_2Cl_2$ sites. The back-transformed spectrum of Figure 7B indicates that a representation of the central feature requires at least two doublets. We have not been able to obtain entirely satisfying fits by making the structurally reasonable assumption that the iron sites of **3** occur in 4:4:2 occupation. A fit for this constrained ratio is shown in Figure 7A, in which the parameters of the four $Fe^{III}N_2Cl_2$ sites have been fixed at $\delta = 0.35$ mm/s and $\Delta E_Q = 1.08$ mm/s. The other values forthcoming from the fit, $\delta = 0.36$ mm/s and $\Delta E_Q = 0.65$ mm/s for four sites and $\delta = 0.28$ mm/s and $\Delta E_Q = 0.64$ mm/s for four sites and $\delta = 0.32$ mm/s and $\Delta E_Q = 0.34$ mm/s for two sites, should be viewed with caution.

The low-temperature Mössbauer spectra of **3**, recorded between 2 and 30 K in applied fields up to 8.0 T are very complex. In low field, and perhaps in high fields as well, the spectra suffer from spin−spin interactions. Moreover, the *g*-anisotropy of the ground electronic doublet shown by EPR suggests that the magnetic hyperfine interactions are anisotropic as well. Further, it is not clear whether the anisotropy of the *g*-values reflects constituents with intrinsically anisotropic *g*-values, as could be expected if the pentacoordinate sites were low spin, or whether these anisotropies reflect mixing of narrowly spaced spin multiplets by zero-field splittings. (The spin-coupled manifolds of **3** comprise 10^6-10^8 microstates, depending on the spin-state assumptions for the pentacoordinate sites.) Mössbauer data, however, reveal that a group of (probably four) iron sites exhibit positive internal magnetic fields ($B_{int} \approx$ 11 T), generally the signature of antiferromagnetic coupling involving high-spin ferric sites. Another group of ca. four iron sites exhibits negative internal fields ($B_{int} \approx -15$ T).

(82) English, D. R.; Hendrickson, D. N.; Suslick, K. S. *Inorg. Chem.* **1983**, *22*, 367−368.

Summary

This work demonstrates that mid-valent molecular iron nitrides of nuclearities 4 and 10 can be prepared by variation of stoichiometry in the self-assembly systems $[FeX_4]^{1-}/(Me_3N)_3Sn$ ($X = Cl^-$, Br^-) in acetonitrile at ambient temperature. The cluster $[Fe_4N_2Cl_{10}]^{4-}$ of overall idealized C_{2h} symmetry, contains a nearly planar, antiferromagnetically coupled $[Fe_4(\mu_3\text{-}N)_2]^{6+}$ core. DFT calculations indicate that the dominant exchange pathway involves pairs of Fe^{III} atoms that are interior and terminal to the Fe_4N_2 rhomboid. The cluster $[Fe_{10}N_8Cl_{12}]^{5-}$, of overall idealized D_{2h} symmetry, is built up by edge- and vertex sharing of 15 Fe_2N_2 rhomboids involving μ_3-N and μ_4-N bridging atoms. The cluster is mixed-valence ($9Fe^{III} + Fe^{IV}$); however, the Fe^{IV} site could not be identified crystallographically or by Mössbauer spectroscopy. It remains to be seen whether the core structures of these clusters are deep thermodynamic sinks, particularly in view of the occurrence of the $[Fe_4(\mu_3\text{-}N)_2]$ grouping in both clusters. The realization of nitride-bridging multiplicities exceeding four and additional cluster topologies remain as synthetic goals in the elaboration of molecular iron nitrides.

Acknowledgment. This research was supported by NIH Grant GM 28856 at Harvard University and by NSF Grant MCB 042 4494 at Carnegie Mellon University. We thank Zachary Shiffler for assistance in collecting Mössbauer spectra.

Supporting Information Available: Crystallographic data for the compounds in Table 1 (in CIF format) and the complete citation of ref 43. This material is available free of charge via the Internet at http://pubs.acs.org.

JA052150L